PHYSICAL REVIEW B **108**, L180102 (2023)

Letter Editors' Suggestion

Physically motivated analytical expression for the temperature dependence of the zero-field splitting of the nitrogen-vacancy center in diamond

M. C. Cambria,[1] G. Thiering,[2] A. Norambuena,[3] H. T. Dinani,[4] A. Gardill,[1] I. Kemeny,[1]
V. Lordi,[5] Á. Gali,[2,6] J. R. Maze,[7,8] and S. Kolkowitz[1,9,*]
[1]Department of Physics, University of Wisconsin, Madison, Wisconsin 53706, USA
[2]HUN-REN Wigner Research Centre for Physics, P.O. Box 49, 1525 Budapest, Hungary
[3]Centro de Optica e Información Cuántica, Universidad Mayor, Camino la Piramide 5750, Huechuraba, Santiago, Chile
[4]Escuela de Ingeniería, Facultad de Ciencias, Ingeniería y Tecnología, Universidad Mayor, Santiago, Chile
[5]Lawrence Livermore National Laboratory, Livermore, California 94551, USA
[6]Department of Atomic Physics, Institute of Physics, Budapest University of Technology and Economics,
Műegyetem rakpart 3, 1111 Budapest, Hungary
[7]Instituto de Física, Pontificia Universidad Católica de Chile, Casilla 306, Santiago, Chile
[8]Centro de Investigación en Nanotecnología y Materiales Avanzados, Pontificia Universidad Católica de Chile, Santiago, Chile
[9]Department of Physics, University of California, Berkeley, California 94720, USA

(Received 8 June 2023; accepted 10 October 2023; published 8 November 2023)

The temperature dependence of the zero-field splitting (ZFS) between the $|m_s = 0\rangle$ and $|m_s = \pm 1\rangle$ levels of the nitrogen-vacancy (NV) center's electronic ground-state spin triplet can be used as a robust nanoscale thermometer in a broad range of environments. However, despite numerous measurements of this dependence in different temperature ranges, to our knowledge no analytical expression has been put forward that captures the scaling of the ZFS of the NV center across all relevant temperatures. Here we present a simple, analytical, and physically motivated expression for the temperature dependence of the NV center's ZFS that matches all experimental observations, in which the ZFS shifts in proportion to the occupation numbers of two representative phonon modes. In contrast to prior models our expression does not diverge outside the regions of fitting. We show that our model quantitatively matches experimental measurements of the ZFS from 15 to 500 K in single NV centers in ultrapure bulk diamond, and we compare our model and measurements to prior models and experimental data.

DOI: 10.1103/PhysRevB.108.L180102

Introduction. The zero-field splitting (ZFS) quantifies the energy difference between a spin system's m_s levels in the absence of externally applied fields. This value plays a critical role in determining the properties of spin defects in crystals, which have emerged as leading platforms for quantum sensing [1–4] and quantum networking [5,6]. Besides characterizing a spin defect's level structure, the ZFS can also be temperature dependent and thereby provides a mechanism for nanoscale thermometry. This effect has already been exploited with the nitrogen-vacancy (NV) center in diamond for *in vivo* thermometry [7–9] and thermal conductivity measurements [10]. In the context of the NV center, the ZFS refers to the splitting between the $m_s = 0$ and $m_s = \pm 1$ levels of the negatively charged NV center's electronic ground-state spin triplet.

The centrality of the ZFS to NV physics and its applications to thermometry has motivated a number of prior works examining its temperature dependence [11–18]. While various analytical expressions have been fitted to the measured NV ZFS temperature dependence over specific temperature ranges, to our knowledge all prior models make use of power series expansions or other approximate polynomial expressions. The utility of these models is somewhat limited by the facts that they diverge outside the range of experimental data used to fit the models and tend to provide little physical insight [12–16]. Recent *ab initio* efforts have demonstrated near quantitative agreement between numerical calculations and experiment, but lack useful analytical expressions [18]. These factors motivate the development of a model of the NV ZFS temperature dependence that is both analytical and physically motivated, such that the model is predictive and practically useful over a wide temperature range, and also provides insight into the spin-lattice interactions that give rise to the temperature dependence.

In this work, we measure the ZFS as a function of temperature in multiple, as-grown, single NV centers in high-purity bulk diamond over a wide range of experimentally relevant temperatures, from 15 to 500 K. We present a novel, simple analytical model of the ZFS temperature dependence in which the ZFS shifts in proportion to the occupation numbers of two representative phonon modes. We provide physical justification for the model by demonstrating that it describes the effects of both first- and second-order atomic displacements. Finally, we discuss the advantages of the proposed model over other currently available models and

---

[*] kolkowitz@berkeley.edu

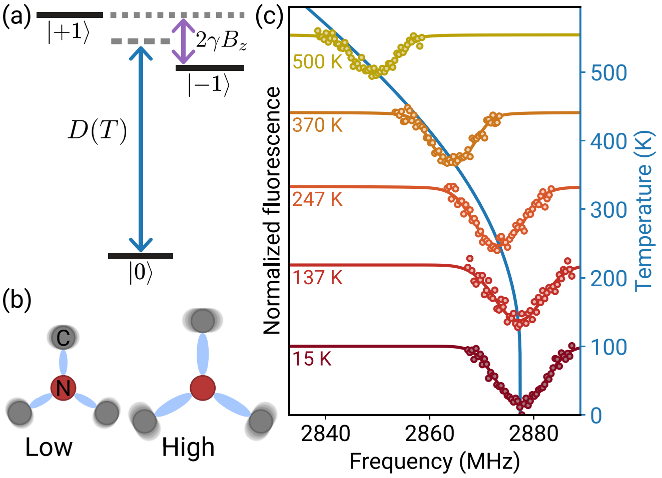

FIG. 1. Temperature-dependent energy levels of the nitrogen-vacancy (NV) center. (a) Electronic ground-state level structure of the negatively charged NV center. In the absence of external fields, the $|m_s = \pm 1\rangle$ spin sublevels are degenerate with energy $D(T)$ above $|m_s = 0\rangle$, where $D(T)$ is the temperature-dependent zero-field splitting (ZFS). The $|\pm 1\rangle$ levels are commonly split by a magnetic field B_z applied along the NV axis. (b) Illustration of the origin of the ZFS temperature dependence. In this 2D diagram, the NV center is projected onto the plane perpendicular to the NV axis, showing only the nitrogen (red) and carbon atoms (gray) nearest the vacancy. The cartoon is not to scale, with the effect of temperature highly exaggerated and only a single vibrational mode depicted for clarity. The ground-state electronic spin density is localized to dangling bonds (blue) between the carbon atoms and the vacancy [19]. Thermal expansion and increases in vibrational amplitudes both reduce the spin-spin interaction that leads to the ZFS [19]. We find that each of these effects can be described by a weighted sum of phonon occupation numbers. (c) Temperature dependence of optically detected magnetic resonance. Data points show fluorescence from a single NV center under zero applied field after optical spin polarization and a microwave pulse at the frequency indicated by the x axis. Solid lines are fits to double-Voigt profiles [20]. Each data set is offset such that the minimum of the fit aligns with the appropriate temperature on the right-hand y axis. The blue line shows the ZFS as a function of temperature according to a fit of the proposed model, Eq. (3), to the full set of experimental data.

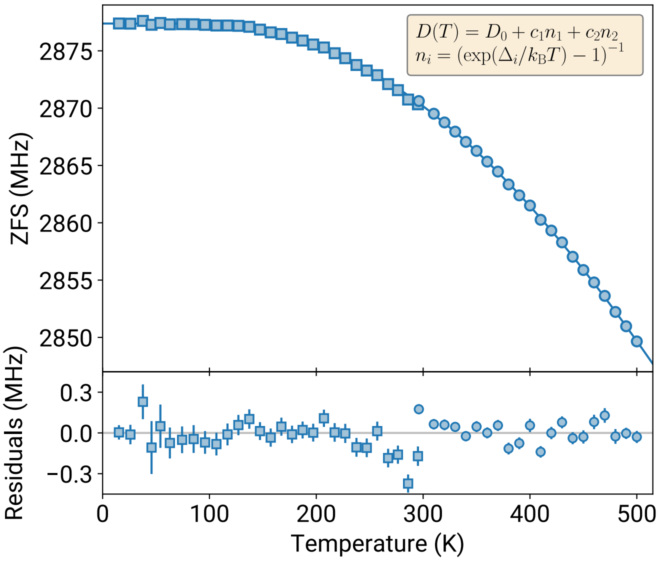

FIG. 2. Zero-field splitting as a function of temperature. Top: Data points show the average zero-field ODMR center frequency of several individual NV centers at each temperature. Square (circle) data points indicate measurements conducted in low- (high-) temperature operation mode using the same 5 NV centers belonging to set A (B). The two sets are mutually exclusive. Standard error bars are smaller than the data points. Solid line shows fit of the proposed model [Eq. (3); reproduced in top right corner] to the experimental data, with fit parameters presented in Table I. Bottom: Residuals.

we highlight the applicability of the proposed model to other spin-lattice effects in spin defects.

Experimental methods. The NV center electronic ground-state level structure is depicted in Fig. 1(a). The ZFS temperature dependence arises due to thermal changes in the positions of the atoms in the crystal lattice [Fig. 1(b)]. An external magnetic field B_z is commonly applied along the NV axis to lift the $|\pm 1\rangle$ degeneracy by $2\gamma B_z$, where $\gamma = 2.8$ MHz/G is the NV gyromagnetic ratio. However, measurements in this work are conducted under no externally applied field. Spectra are recorded using a pulsed optically detected magnetic resonance (ODMR) sequence [Fig. 1(c)], and the ZFS is recorded as the center frequency of the fit to each spectrum [20]. The experimental apparatus is similar to that described in Ref. [21]. The apparatus features dual low- and high-temperature operation modes where the sample temperature is monitored by a resistance temperature detector (RTD) mounted immediately adjacent to the diamond sample. Experiments were conducted using two sets of NV centers within the same high-purity bulk diamond sample ([NV] $\sim 10^{-3}$ ppb). Low-temperature measurements were conducted with 5 single NV centers comprising set A at temperatures between 15 and 295 K. Unfortunately, after switching from low-temperature to high-temperature operation we were unable to relocate the region with the NV centers in set A. High-temperature measurements were therefore conducted with 5 single NV centers in a different region comprising set B at temperatures between 296 and 500 K. NVs belonging to the same set are within approximately 100 microns of each other, and are over 10 microns below the diamond surface. The two sets are mutually exclusive and from different regions of the diamond. Further experimental details are available in the Supplemental Material [20].

Results. Figure 2 shows the average ZFS recorded for the NV centers belonging to each set (set A, squares; set B, circles) as a function of temperature. For reasons that we detail below, a model of the form

$$D(T) = D_0 + \sum_{i=1}^{M} c_i n_i \tag{1}$$

provides an excellent fit to the experimental data. Here, $D(T)$ is the ZFS at temperature T and D_0 is the ZFS at 0 K. The model includes M discrete phonon modes indexed by i. Intuitively, each c_i describes how the corresponding phonon mode shifts the ZFS by modulating the mean positions and vibrational amplitudes of the atoms in the lattice. The mean occupation number of the ith

TABLE I. Fit parameters for the ZFS temperature dependence according to the model described by Eq. (3). Values are reported to at least 4 significant figures. Uncertainties are 1σ.

D_0 (MHz)	c_1 (MHz)	Δ_1 (meV)	c_2 (MHz)	Δ_2 (meV)
2877.38 ± 0.03	-54.91 ± 7.35	58.73 ± 2.32	-249.6 ± 19.4	145.5 ± 8.4

mode is

$$n_i = \frac{1}{e^{\Delta_i/k_B T} - 1}, \tag{2}$$

where Δ_i is the mode energy and k_B is the Boltzmann constant. The sum over i in Eq. (1) may be restricted to a small number of representative phonon modes with coefficients that absorb the effects of other modes with similar energies. We find that including just $M = 2$ representative phonon modes is sufficient to fully capture the behavior of the ZFS over the entire temperature range measured in this and prior works [20], resulting in the simple analytical expression

$$D(T) = D_0 + c_1 n_1 + c_2 n_2. \tag{3}$$

We fit Eq. (3) to the data with the quantities D_0, $c_{1,2}$, and $\Delta_{1,2}$ as free parameters. The values extracted from the fit are presented in Table I. The energies of the two phonon modes as determined by the fit are $\Delta_1 = 58.73 \pm 2.32$ meV and $\Delta_2 = 145.5 \pm 8.4$ meV, roughly consistent with the highest energies of specific acoustic and optical phonon branches in diamond, at approximately 70 and 165 meV, respectively [22]. The representative mode energies also coincide with those found to dominate spin-phonon relaxation [21] and the NV optical phonon sideband [23–26]. Further comparison of the phonon energies identified here and in other contexts is available in Sec. VI of the Supplemental Material [20].

The fit residuals are consistent with statistical uncertainties over most of the measured temperature range (Fig. 2, bottom). Larger residuals arise near room temperature where the measured ZFS values from sets A and B were found to be offset from each other by approximately 300 kHz. The low-temperature measurements made in this work are similarly approximately 300 kHz below those reported by Chen *et al.* and Li *et al.* in Refs. [12,15]. This offset with respect to prior data sets is constant across the full temperature range probed for set A NV centers in this work (15 to 295 K). The weak temperature dependence of the ZFS at low temperatures suggests that the offset may be the result of a small but real physical effect, and is likely not the result of a systematic error in measurement. A survey of room-temperature ODMR spectra in different regions of the diamond sample used in this work evidences small environmental variations over length scales of hundreds of microns. We tentatively suggest that the set A NV centers are in a region of relatively high strain, leading to the 300 kHz offset in the average ZFS. The results of the survey and further analysis are available in Sec. III of the Supplemental Material [20].

Discussion. We now turn to a discussion of the physical origins of Eq. (1). For a generic solid-state spin system, changes in temperature affect the positions of atoms in the solid which in turn modulate the system's electronic wave function, leading the ZFS to acquire a temperature dependence. Recent *ab initio* work has achieved near-quantitative agreement with experimental measurements of the NV ZFS temperature dependence by accounting for the second-order effects of atomic displacements in addition to the effect of thermal expansion in a 64-atom supercell [18]. Here we adopt a similar premise as a starting point, writing the ZFS as a series expansion about the atomic displacements relative to their equilibrium positions at 0 K and evaluating the time average of the series at a given temperature. With D_ℓ indicating the contribution to the ZFS at the ℓth order in the atomic displacements,

$$D(T) = D_0 + D_1 + D_2 + \cdots . \tag{4}$$

As in Eq. (1), D_0 is the ZFS at zero temperature. The linear term is given by

$$D_1 = \sum_{j\mu} \frac{\partial D}{\partial u_{j\mu}^{(0)}} \langle u_{j\mu}^{(0)} \rangle, \tag{5}$$

where $\langle \cdot \rangle$ indicates the time average at temperature T and $u_{j\mu}^{(0)}$ is the displacement of the jth atom in the lattice relative to its equilibrium position at 0 K along the μ axis. The quadratic term is given by

$$D_2 = \frac{1}{2} \sum_{jj'\mu\mu'} \frac{\partial^2 D}{\partial u_{j\mu}^{(0)} \partial u_{j'\mu'}^{(0)}} \langle u_{j\mu}^{(0)} u_{j'\mu'}^{(0)} \rangle. \tag{6}$$

Higher-order terms are anticipated to be negligible on general grounds. As we explain below, both the first-order and second-order contributions can be written as a weighted sum over a small number of mean phonon occupation numbers, ultimately yielding the proposed model given by Eq. (1).

Beginning with the first-order contributions, the time-averaged atomic displacements may be related to the deviation of the lattice constant from its zero-temperature limit using a set of geometric proportionality constants. That is,

$$\langle u_{j\mu}^{(0)} \rangle = \beta_{j\mu}[a(T) - a_0], \tag{7}$$

where $a(T)$ and a_0 denote the lattice constant at temperature T and 0 K, respectively, and the $\beta_{j\mu}$ are the geometric proportionality constants. The lattice constant changes with temperature according to

$$a(T) = a_0 \exp\left[\int_0^T \alpha(T)\, dT\right], \tag{8}$$

where $\alpha(T)$ is the coefficient of thermal expansion. To obtain an expression for this quantity, we adopt the quasiharmonic approximation, in which the crystal's phonon modes are assumed to have volume-dependent frequencies but are otherwise treated harmonically [18,28]. The quasiharmonic approximation is widely used to account for thermal expansion in crystals, where the coefficient of thermal expansion is [28]

$$\alpha(T) = -\frac{\hbar}{3B} \sum_{k\nu} \frac{\partial \omega_{k\nu}}{\partial V} \frac{\partial n_{k\nu}}{\partial T}. \tag{9}$$

Here, the kth phonon mode with polarization ν has energy $\hbar\omega_{k\nu}$ and mean occupation number $n_{k\nu}$. The bulk modulus and volume are denoted B and V, respectively. The frequency derivatives $\partial\omega_{k\nu}/\partial V$ are closely related to the Grüneisen parameters that appear in the quasiharmonic model of thermal expansion [29,30]. Integrating Eq. (8) and neglecting the weak temperature dependence of the bulk modulus, the argument of the exponential becomes a weighted sum over mean occupation numbers. After expanding the exponential and dropping higher-order terms we obtain

$$a(T) \approx a_0\left(1 + \sum_{k\nu} \rho_{k\nu} n_{k\nu}\right), \tag{10}$$

where $\rho_{k\nu} = -(\hbar/3B)(\partial\omega_{k\nu}/\partial V)$. As with Eq. (1), we find a sum over just two representative phonon modes displays excellent agreement with measurements of the lattice constant as a function of temperature. Reduced to two modes, Eq. (10) becomes

$$a(T) \approx a_0 + b_1 n_1 + b_2 n_2. \tag{11}$$

Here, as in Eq. (3), the subscripts 1 and 2 index two representative modes. To demonstrate the accuracy of this model, we fit Eq. (11) to a set of lattice constant data generated from the results of Ref. [27], which matches experimental measurements of the diamond lattice constant [20]. We fix the representative mode energies to those extracted from the ZFS temperature dependence fit, $\Delta_1 = 58.73$ meV and $\Delta_2 = 145.5$ meV. We treat the zero-temperature lattice constant a_0 and the coefficients $b_{1,2}$ as fit parameters. As shown in Fig. 3(a), Eq. (11) provides an excellent description of the diamond lattice constant with only three free parameters. Over the fit range of 0 to 1000 K, the maximal difference between the two curves is just 9 μÅ, or 0.11% of the change in the lattice constant between 0 and 1000 K. The first-order contribution to the NV ZFS temperature dependence is therefore well approximated as

$$D_1 \approx c_1' n_1 + c_2' n_2, \tag{12}$$

where the $c_{1,2}'$ are here simply interpreted as unknown weights.

We next show that the second-order contribution to the ZFS can similarly be expressed as a weighted sum over occupation numbers in the quasiharmonic model. First, we define new displacement coordinates that are relative to the equilibrium atomic positions at a given temperature. The new coordinates are

$$u_{j\mu} = u_{j\mu}^{(0)} - \langle u_{j\mu}^{(0)} \rangle. \tag{13}$$

Writing Eq. (6) in terms of the $u_{j\mu}$ yields

$$D_2 = \frac{1}{2} \sum_{jj'\mu\mu'} \frac{\partial^2 D}{\partial u_{j\mu}\partial u_{j'\mu'}} \left(\langle u_{j\mu} u_{j'\mu'} \rangle + \langle u_{j\mu}^{(0)} \rangle \langle u_{j'\mu'}^{(0)} \rangle\right), \tag{14}$$

where we have used $\langle u_{j\mu} \rangle = 0$. We drop the latter product of thermal expansion terms, $\langle u_{j\mu}^{(0)} \rangle \langle u_{j'\mu'}^{(0)} \rangle$, which are expected to provide negligible contributions to the ZFS for a system with a highly localized wave function in a weakly anharmonic lattice. Transforming to the basis of normal coordinates $q_{k\nu}$ for a harmonic lattice [28],

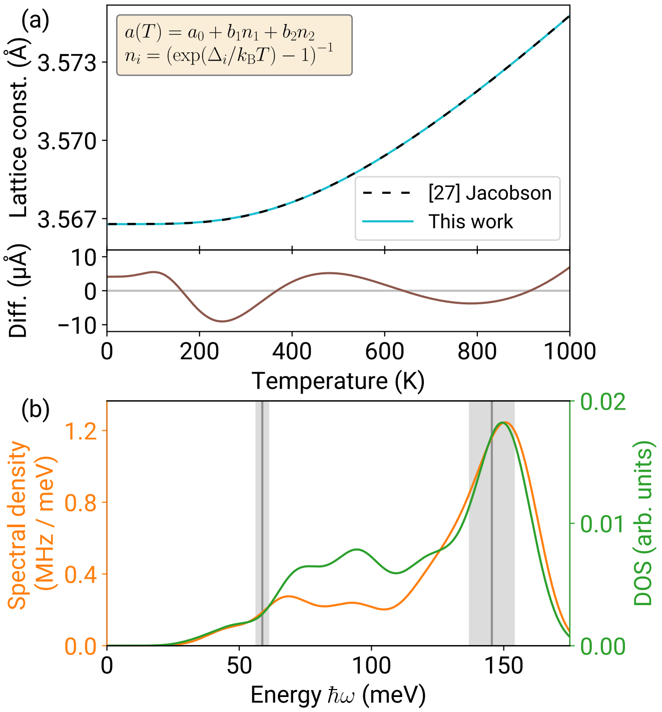

FIG. 3. Physical motivation for proposed model of the zero-field splitting temperature dependence. (a) Diamond lattice constant as a function of temperature. Dashed black line indicates the diamond lattice constant calculated from the results of Ref. [27]. Fitting Eq. (11) (reproduced in upper left corner) to this curve yields an excellent approximation of the lattice constant with just three free parameters (cyan line). The form of Eq. (11) matches that of Eq. (3). Bottom: Residuals. (b) Second-order spin-phonon spectral density (orange) and phonon density of states (DOS; green) calculated from the results of Ref. [21]. The spectral density describes the shift of the ZFS induced by the second-order effects of phonons at a given energy. The spectral density closely matches the DOS, suggesting that both first- and second-order contributions to ZFS shifts can be modeled by a weighted sum of occupation numbers of phonon modes with representative energies. The energies extracted from the fit of Eq. (3) to the experimental ZFS data (gray lines and ±1σ intervals) roughly match the locations of prominent features in the spectral density and DOS. Note that the spectral density is negative everywhere. The plot shows its magnitude.

$$D_2 = \frac{1}{2} \sum_{kk'\nu\nu'} \frac{\partial^2 D}{\partial q_{k\nu}\partial q_{k'\nu'}} \langle q_{k\nu} q_{k'\nu'} \rangle. \tag{15}$$

Because phonon modes in the quasiharmonic approximation are noninteracting at a given temperature, the time average of the cross terms is zero. Each of the remaining terms $\langle q_{k\nu}^2 \rangle$ is proportional to the mode occupation number $n_{k\nu}$ plus a zero-point contribution that may be absorbed by the constant term D_0 [18]. Thus we can write

$$D_2 = \sum_{k\nu} \lambda_{k\nu} n_{k\nu}, \tag{16}$$

where the $\lambda_{k\nu}$ are second-order spin-phonon coupling coefficients proportional to the second derivatives in Eq. (15). In the continuum limit, the coupling coefficients are replaced by

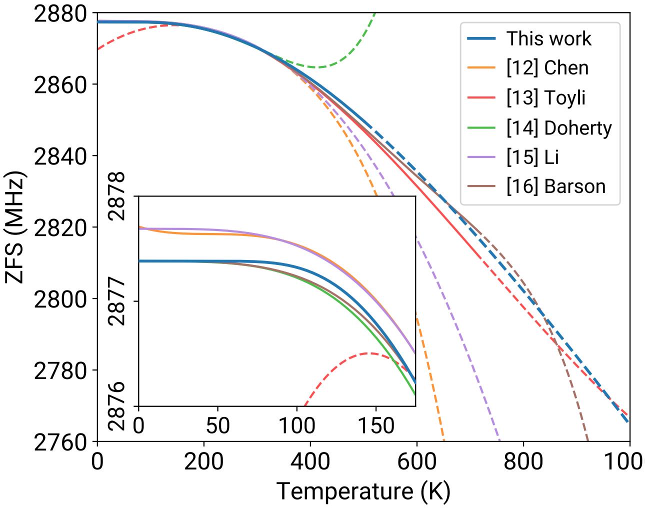

FIG. 4. Comparison to prior models of the ZFS temperature dependence. Prior models are reproduced from Refs. [12–16] according to the fit parameters published in those works. The line for each model turns from solid to dashed outside the temperature range covered by the experimental data on which the model was fit. See Sec. IV of the Supplemental Material for details regarding prior results [20]. Inset: Low-temperature behavior of models.

the second-order spin-phonon spectral density $S_2(\hbar\omega)$ defined such that

$$D_2 = \int S_2(\hbar\omega)\, n(\hbar\omega)\, d(\hbar\omega), \tag{17}$$

where $n(\hbar\omega)$ is the mean occupation number at energy $\hbar\omega$. The spectral density and phonon density of states according to the NV center supercell calculations described in Ref. [21] are reproduced in Fig. 3(b) as the orange and green lines, respectively. In Ref. [21], it was shown that NV center spin-phonon relaxation can be reproduced by replacing this spectral density with two representative phonon modes, and we take the same approach here. The similarity between the spectral density and the density of states indicates that this may be done most effectively by retaining the modes associated with a large density of states. Because such modes are also good representative modes for the diamond lattice constant, we expect that the second-order contributions to the ZFS can be expressed by considering the same two representative modes used to describe the first-order contribution as given in Eq. (12). Therefore we have

$$D_2 \approx c_1'' n_1 + c_2'' n_2, \tag{18}$$

where the coefficients $c_{1,2}''$ are again unknown weights. Finally combining the contributions up to second order yields

$$D(T) \approx D_0 + (c_1' + c_1'')n_1 + (c_2' + c_2'')n_2, \tag{19}$$

and substituting $c_{1,2} = c_{1,2}' + c_{1,2}''$, we arrive at Eq. (3).

In Fig. 4 we compare our model of the ZFS temperature dependence to models from prior literature that were fitted to experimental data spanning a temperature range of at least 100 K. For clarity, the experimental data from the prior works is not shown in the main text plot, but is available in the Supplemental Material [20]. The NV center has been coherently manipulated at temperatures up to approximately 1000 K [31], so we treat 0–1000 K as the full experimentally relevant temperature range. Each model provides a good description of the data on which it was fitted (solid regions of lines in Fig. 4), but diverges at either high or low temperatures beyond the range covered by the data, which is characteristic of power series [12,13] and related expressions [14–16]. In contrast, the model presented in this work provides reasonable predictions of the ZFS even well beyond the experimental temperature range of 15–500 K. We provide more detailed direct comparisons between the different models in Sec. IV of the Supplemental Material, including direct comparisons between the various models when fitted to our new data set [20].

The available experimental data sets somewhat disagree with each other in several limits. As discussed above, the low-temperature ZFS values measured for this work are approximately 300 kHz lower than those presented in Refs. [12] and [15]. The results of Refs. [13] and [17] and our own set B measurements are in good agreement under ambient conditions, but exhibit slightly different temperature scalings such that the three data sets disagree with each other by several hundred kHz at 400 K [20]. This is most likely due to systematic temperature differentials between the diamond and the temperature sensor in two or potentially all three experiments. A detailed description of how temperature was determined in this work is provided in Sec. I of the Supplemental Material [20]. Despite these differences, we emphasize that the ZFS temperature dependence model presented in this work [Eq. (3)] can fully describe all of the available experimental data sets even if the energies of the representative modes are held fixed to the values reported in Table I, 58.73 and 145.5 meV [20].

While our measurements were performed on single NV centers in bulk diamond, we expect that the functional form of the model of the ZFS temperature dependence presented here should be applicable to high-density ensembles of NV centers, near-surface NV centers, and NV centers in nanodiamonds, as the characteristic wavelengths of the representative phonon modes are both below 1 nm. Besides providing a more practical expression for the ZFS temperature dependence, our model may also provide important insights into other properties that derive from interactions between the NV defect and the crystal lattice. Noting that the optical zero-phonon line wavelength [12,14], hyperfine coupling strengths [17,32], and excited state zero-field splitting [33,34] depend on temperature in a way that is qualitatively similar to the ZFS temperature dependence, we suggest that expressions similar to Eq. (3) could be derived for these properties. Similar models could also be developed for other defect systems, such as divacancy centers in silicon carbide [35] or vacancies in 2D materials [36].

Conclusion. In this work we have presented measurements of the ground-state zero-field splitting (ZFS) in single NV centers in high-purity bulk diamond sample from 15 to 500 K. Our analytical model for the NV ZFS, which describes the shift as proportional to the occupation numbers of two representative phonon modes, is in excellent agreement with the experimental data. We explained the physical origins of our model, and suggested that it could replace the power series commonly employed in other works. Finally, we suggested that this model may be readily adapted to several other important properties of the NV center and to other solid-state defects.

Acknowledgments. We gratefully acknowledge Hao Tang, Ariel Rebekah Barr, and Guoqing Wang for enlightening conversations, and Peter Maurer for helpful feedback on our manuscript. Experimental work, data analysis, and theoretical efforts conducted at UW-Madison were supported by the U.S. Department of Energy, Office of Science, Basic Energy Sciences, under Award No. DE-SC0020313. Part of this work by V.L. was performed under the auspices of the U.S. Department of Energy at Lawrence Livermore National Laboratory under Contract No. DE-AC52-07NA27344. A.N. acknowledges financial support from Fondecyt Iniciación No. 11220266. A.G. acknowledges support from the Department of Defense through the National Defense Science and Engineering Graduate Fellowship (NDSEG) program. Á.G. acknowledges support from the NKFIH in Hungary for the National Excellence Program (Grant No. KKP129866), the Quantum Information National Laboratory (Grant No. 2022-2.1.1-NL-2022-00004), and the EU QuantERA II MAESTRO project, and from the European Commission for the QuMicro project (Grant No. 101046911). G.T. was supported by the János Bolyai Research Scholarship of the Hungarian Academy of Sciences. Á.G. and G.T. acknowledge the high-performance computational resources provided by KIFÜ (Governmental Agency for IT Development) Institute of Hungary. J.R.M. acknowledges support from ANID-Fondecyt Grant No. 1221512 and ANID-Anillo Grant No. ACT192023.

---

[1] J. M. Abendroth, K. Herb, E. Janitz, T. Zhu, L. A. Völker, and C. L. Degen, Single-nitrogen–vacancy NMR of amine-functionalized diamond surfaces, Nano Lett. **22**, 7294 (2022).

[2] Z. Qiu, A. Hamo, U. Vool, T. X. Zhou, and A. Yacoby, Nanoscale electric field imaging with an ambient scanning quantum sensor microscope, npj Quantum Inf. **8**, 107 (2022).

[3] Y. Chen, C. Li, T. Yang, E. A. Ekimov, C. Bradac, S. T. Ha, M. Toth, I. Aharonovich, and T. T. Tran, Real-time ratiometric optical nanoscale thermometry, ACS Nano **17**, 2725 (2023).

[4] J. Rovny, Z. Yuan, M. Fitzpatrick, A. I. Abdalla, L. Futamura, C. Fox, M. C. Cambria, S. Kolkowitz, and N. P. de Leon, Nanoscale covariance magnetometry with diamond quantum sensors, Science **378**, 1301 (2022).

[5] C. Bradley, S. de Bone, P. Möller, S. Baier, M. Degen, S. Loenen, H. Bartling, M. Markham, D. Twitchen, R. Hanson *et al.*, Robust quantum-network memory based on spin qubits in isotopically engineered diamond, npj Quantum Inf. **8**, 122 (2022).

[6] P.-J. Stas, Y. Q. Huan, B. Machielse, E. N. Knall, A. Suleymanzade, B. Pingault, M. Sutula, S. W. Ding, C. M. Knaut, D. R. Assumpcao *et al.*, Robust multi-qubit quantum network node with integrated error detection, Science **378**, 557 (2022).

[7] G. Kucsko, P. C. Maurer, N. Y. Yao, M. Kubo, H. J. Noh, P. K. Lo, H. Park, and M. D. Lukin, Nanometre-scale thermometry in a living cell, Nature (London) **500**, 54 (2013).

[8] M. Fujiwara, S. Sun, A. Dohms, Y. Nishimura, K. Suto, Y. Takezawa, K. Oshimi, L. Zhao, N. Sadzak, Y. Umehara *et al.*, Real-time nanodiamond thermometry probing in vivo thermogenic responses, Sci. Adv. **6**, eaba9636 (2020).

[9] J. Choi, H. Zhou, R. Landig, H.-Y. Wu, X. Yu, S. E. Von Stetina, G. Kucsko, S. E. Mango, D. J. Needleman, A. D. Samuel *et al.*, Probing and manipulating embryogenesis via nanoscale thermometry and temperature control, Proc. Natl. Acad. Sci. USA **117**, 14636 (2020).

[10] A. Laraoui, H. Aycock-Rizzo, Y. Gao, X. Lu, E. Riedo, and C. A. Meriles, Imaging thermal conductivity with nanoscale resolution using a scanning spin probe, Nat. Commun. **6**, 8954 (2015).

[11] V. M. Acosta, E. Bauch, M. P. Ledbetter, A. Waxman, L.-S. Bouchard, and D. Budker, Temperature dependence of the nitrogen-vacancy magnetic resonance in diamond, Phys. Rev. Lett. **104**, 070801 (2010).

[12] X.-D. Chen, C.-H. Dong, F.-W. Sun, C.-L. Zou, J.-M. Cui, Z.-F. Han, and G.-C. Guo, Temperature dependent energy level shifts of nitrogen-vacancy centers in diamond, Appl. Phys. Lett. **99**, 161903 (2011).

[13] D. M. Toyli, D. J. Christle, A. Alkauskas, B. B. Buckley, C. G. Van de Walle, and D. D. Awschalom, Measurement and control of single nitrogen-vacancy center spins above 600 K, Phys. Rev. X **2**, 031001 (2012).

[14] M. W. Doherty, V. M. Acosta, A. Jarmola, M. S. J. Barson, N. B. Manson, D. Budker, and L. C. L. Hollenberg, Temperature shifts of the resonances of the NV^- center in diamond, Phys. Rev. B **90**, 041201(R) (2014).

[15] C.-C. Li, M. Gong, X.-D. Chen, S. Li, B.-W. Zhao, Y. Dong, G.-C. Guo, and F.-W. Sun, Temperature dependent energy gap shifts of single color center in diamond based on modified Varshni equation, Diam. Relat. Mater. **74**, 119 (2017).

[16] M. S. J. Barson, P. Reddy, S. Yang, N. B. Manson, J. Wrachtrup, and M. W. Doherty, Temperature dependence of the ^{13}C hyperfine structure of the negatively charged nitrogen-vacancy center in diamond, Phys. Rev. B **99**, 094101 (2019).

[17] S. Lourette, A. Jarmola, V. M. Acosta, A. G. Birdwell, D. Budker, M. W. Doherty, T. Ivanov, and V. S. Malinovsky, Temperature sensitivity of $^{14}\mathrm{N}\text{-}V$ and $^{15}\mathrm{N}\text{-}V$ ground-state manifolds, Phys. Rev. Appl. **19**, 064084 (2023).

[18] H. Tang, A. R. Barr, G. Wang, P. Cappellaro, and J. Li, First-principles calculation of the temperature-dependent transition energies in spin defects, J. Phys. Chem. Lett. **14**, 3266 (2023).

[19] Á. Gali, Ab initio theory of the nitrogen-vacancy center in diamond, Nanophotonics **8**, 1907 (2019).

[20] See Supplemental Material at http://link.aps.org/supplemental/10.1103/PhysRevB.108.L180102 for additional experimental and theoretical details, which includes Refs. [37–48].

[21] M. Cambria, A. Norambuena, H. T. Dinani, G. Thiering, A. Gardill, I. Kemeny, Y. Li, V. Lordi, Á. Gali, J. R. Maze, and S. Kolkowitz, Temperature-dependent spin-lattice relaxation of the nitrogen-vacancy spin triplet in diamond, Phys. Rev. Lett. **130**, 256903 (2023).

[22] P. Pavone, K. Karch, O. Schütt, D. Strauch, W. Windl, P. Giannozzi, and S. Baroni, *Ab initio* lattice dynamics of diamond, Phys. Rev. B **48**, 3156 (1993).

[23] G. Davies, Vibronic spectra in diamond, J. Phys. C **7**, 3797 (1974).

[24] A. Collins, M. Stanley, and G. Woods, Nitrogen isotope effects in synthetic diamonds, J. Phys. D **20**, 969 (1987).

[25] P. Kehayias, M. W. Doherty, D. English, R. Fischer, A. Jarmola, K. Jensen, N. Leefer, P. Hemmer, N. B. Manson, and D. Budker, Infrared absorption band and vibronic structure of the nitrogen-vacancy center in diamond, Phys. Rev. B **88**, 165202 (2013).

[26] A. Alkauskas, B. B. Buckley, D. D. Awschalom, and C. G. Van de Walle, First-principles theory of the luminescence lineshape for the triplet transition in diamond NV centres, New J. Phys. **16**, 073026 (2014).

[27] P. Jacobson and S. Stoupin, Thermal expansion coefficient of diamond in a wide temperature range, Diam. Relat. Mater. **97**, 107469 (2019).

[28] N. W. Ashcroft and N. D. Mermin, *Solid State Physics* (Holt, Rinehart and Winston, New York, 1976).

[29] M. Blackman, On the thermal expansion of solids, Proc. Phys. Soc., Sect. B **70**, 827 (1957).

[30] R. R. Reeber, Thermal expansion of some group IV elements and ZnS, Phys. Status Solidi A **32**, 321 (1975).

[31] G.-Q. Liu, X. Feng, N. Wang, Q. Li, and R.-B. Liu, Coherent quantum control of nitrogen-vacancy center spins near 1000 kelvin, Nat. Commun. **10**, 1344 (2019).

[32] S. Xu, M. Liu, T. Xie, Z. Zhao, Q. Shi, P. Yu, C.-K. Duan, F. Shi, and J. Du, High-precision measurements and first-principles explanation of the temperature-dependent ^{13}C and ^{14}N hyperfine interactions of single NV$^-$ centers in diamond at room temperature, Phys. Rev. B **107**, L140101 (2023).

[33] G. D. Fuchs, V. V. Dobrovitski, R. Hanson, A. Batra, C. D. Weis, T. Schenkel, and D. D. Awschalom, Excited-state spectroscopy using single spin manipulation in diamond, Phys. Rev. Lett. **101**, 117601 (2008).

[34] P. Neumann, R. Kolesov, V. Jacques, J. Beck, J. Tisler, A. Batalov, L. Rogers, N. Manson, G. Balasubramanian, F. Jelezko *et al.*, Excited-state spectroscopy of single NV defects in diamond using optically detected magnetic resonance, New J. Phys. **11**, 013017 (2009).

[35] W.-X. Lin, F.-F. Yan, Q. Li, J.-f. Wang, Z.-H. Hao, J.-Y. Zhou, H. Li, L.-X. You, J.-S. Xu, C.-F. Li, and G. C. Guo, Temperature dependence of divacancy spin coherence in implanted silicon carbide, Phys. Rev. B **104**, 125305 (2021).

[36] W. Liu, Z.-P. Li, Y.-Z. Yang, S. Yu, Y. Meng, Z.-A. Wang, Z.-C. Li, N.-J. Guo, F.-F. Yan, Q. Li *et al.*, Temperature-dependent energy-level shifts of spin defects in hexagonal boron nitride, ACS Photon. **8**, 1889 (2021).

[37] Z. Wang, J. Zhang, X. Feng, and L. Xing, Microwave heating effect on diamond samples of nitrogen-vacancy centers, ACS Omega **7**, 31538 (2022).

[38] K. Ouyang, Z. Wang, L. Xing, X. Feng, J. Zhang, C. Ren, and X. Yang, Temperature dependence of the zero-field splitting parameter of nitrogen-vacancy centre ensembles in diamond considering microwave and laser heating effect, Meas. Sci. Technol. **34**, 015102 (2023).

[39] D. A. Broadway, B. Johnson, M. Barson, S. E. Lillie, N. Dontschuk, D. McCloskey, A. Tsai, T. Teraji, D. Simpson, A. Stacey *et al.*, Microscopic imaging of the stress tensor in diamond using in situ quantum sensors, Nano Lett. **19**, 4543 (2019).

[40] P. Kehayias, M. J. Turner, R. Trubko, J. M. Schloss, C. A. Hart, M. Wesson, D. R. Glenn, and R. L. Walsworth, Imaging crystal stress in diamond using ensembles of nitrogen-vacancy centers, Phys. Rev. B **100**, 174103 (2019).

[41] M. C. Marshall, R. Ebadi, C. Hart, M. J. Turner, M. J. H. Ku, D. F. Phillips, and R. L. Walsworth, High-precision mapping of diamond crystal strain using quantum interferometry, Phys. Rev. Appl. **17**, 024041 (2022).

[42] T. Mittiga, S. Hsieh, C. Zu, B. Kobrin, F. Machado, P. Bhattacharyya, N. Z. Rui, A. Jarmola, S. Choi, D. Budker, and N. Y. Yao, Imaging the local charge environment of nitrogen-vacancy centers in diamond, Phys. Rev. Lett. **121**, 246402 (2018).

[43] T. Sato, K. Ohashi, T. Sudoh, K. Haruna, and H. Maeta, Thermal expansion of a high purity synthetic diamond single crystal at low temperatures, Phys. Rev. B **65**, 092102 (2002).

[44] M. W. Doherty, V. V. Struzhkin, D. A. Simpson, L. P. McGuinness, Y. Meng, A. Stacey, T. J. Karle, R. J. Hemley, N. B. Manson, L. C. L. Hollenberg, and S. Prawer, Electronic properties and metrology applications of the diamond NV$^-$ center under pressure, Phys. Rev. Lett. **112**, 047601 (2014).

[45] R. R. Reeber and K. Wang, Thermal expansion, molar volume and specific heat of diamond from 0 to 3000 K, J. Electron. Mater. **25**, 63 (1996).

[46] A. Rohatgi, Webplotdigitizer, Version 4.6, https://automeris.io/WebPlotDigitizer.

[47] A. Bosak and M. Krisch, Phonon density of states probed by inelastic x-ray scattering, Phys. Rev. B **72**, 224305 (2005).

[48] S. Stoupin and Y. V. Shvyd'ko, Thermal expansion of diamond at low temperatures, Phys. Rev. Lett. **104**, 085901 (2010).